Boletim da Sociedade Astronômica Brasileira, **37**, no. 1, 375-379

A study of the star clusters Berkeley 27, Collinder 104, Collinder 106, and NGC 2301 in the Monoceros region using GAIA DR3 and Strömgren photometry with SOAR

Thomas M. dos Santos[1], Wagner J. B. Corradi[1,2], Francisco F. S. Maia[4], Nadia Kaltcheva[5], Filipe A. Ferreira[1], João F. C. Santos Jr.[1], Mateus S. Angelo[3]

[1] Universidade Federal de Minas Gerais e-mail: thomas.miler.dos.santos@gmail.com, jsantos@fisica.ufmg.br, filipe1906@ufmg.br
[2] Laboratório Nacional de Astrofísica e-mail: wbcorradi@lna.br
[3] Centro Federal de Educação Tecnológica de Minas Gerais e-mail: mateusangelo@cefetmg.br
[4] Universidade Federal do Rio de Janeiro e-mail: ffsmaia@if.ufrj.br
[5] University of Wisconsin Oshkosh e-mail: kaltchev@uwosh.edu

Abstract. Monoceros, located in the Milky Way's Perseus Arm, is a promising star-forming region featuring open clusters, H II regions, interstellar clouds, and emission nebulae, providing valuable opportunities to study the interactions between young stars and their environment. This study presents Strömgren uvby photometric data from the SOAR Telescope for clusters Collinder 104, Collinder 106, Berkeley 27, and NGC 2301. Using Gaia DR3 data, we determined parallax, proper motion, membership, age, extinction, metallicity, distance, and radii. For the first time, masses have been calculated for these clusters. Combining SOAR and Gaia data, we derived reddening-free indices and used the $m_1(b-y)$ metallicity index to refine the cluster's parameters. These results shed light on Monoceros' star formation history and its role in Galactic dynamics.

Resumo. Monoceros, localizada no Braço de Perseus da Via Láctea, é uma região promissora de formação estelar que apresenta aglomerados abertos, regiões HII, nuvens interestelares e nebulosas de emissão, oferecendo valiosas oportunidades para o estudo das interações entre estrelas jovens e seu ambiente. Este estudo apresenta dados fotométricos de Strömgren uvby obtidos com o Telescópio SOAR para os aglomerados Collinder 104, Collinder 106, Berkeley 27 e NGC 2301. Utilizando dados do Gaia DR3, determinamos paralaxe, movimento próprio, associação (membership), idade, extinção, metalicidade, distância e raios. Pela primeira vez, foram calculadas as massas desses aglomerados. Combinando dados do SOAR e do Gaia, derivamos índices livres de avermelhamento e utilizamos o índice de metalicidade $m_1(b-y)$ para refinar os parâmetros dos aglomerados. Esses resultados lançam luz sobre a história de formação estelar de Monoceros e seu papel na dinâmica Galáctica.

Keywords. open clusters and associations: general – Galaxy: stellar content – Surveys, mass

1. Introduction

Open clusters play a crucial role in characterizing the Galaxy's disk and are essential to study stellar evolution. Such stellar population units are coeval in terms of age, metallicity, distance, and kinematics but diverse in terms of stellar masses Krumholz et al. (2019).

As new clusters are discovered and characterized, our understanding of the Galactic structure, its chemical dynamics, and evolution expands significantly.

The present work makes use of astrometric and photometric data from the Gaia DR3 mission to derive astrophysical parameters for the clusters studied. It also incorporates $uvby$ photometric data collected with the SOAR telescope to obtain the reddening-free indices (e.g. Piatti et al. (2019)). Additionally, we apply the relation from Casagrande et al. (2011) to derive the $m_1(b-y)$ indices and metallicities $[Fe/H]$ for the clusters Berkeley 27, Collinder 104, Collinder 106, and NGC 2301.

1.1. Monoceros Region

Monoceros is located in the Perseus Arm of the Milky Way, near the Galactic coordinates $213° < l < 200°$ and $-3° < b < 3°$. The region is characterized by the presence of several open clusters, HII regions, molecular clouds, and emission nebulae (e.g. Hunt & Reffert (2023); Tarricq et al. (2022); Dias et al. (2021); Jaehnig et al. (2021); Kaltcheva et al. (2010). These structures indicate ongoing star formation, making Monoceros a particularly suitable laboratory for investigating the connection between young stellar populations and the interstellar medium, as well as for probing the structure of the Galactic disk toward the anticentre. See Figure 1.

1.2. GOALS

- To determine the astrophysical and structural parameters of the open clusters using Gaia DR3 data;
- To derive the metallicity through Strömgren photometry;
- To investigate correlations among the clusters and between the clusters and the interstellar medium.

2. Methodology & Results

2.1. GAIA DR3

This section describes the methodology adopted for the analysis of all the clusters studied, based on **Gaia DR3** data. The individual steps of the procedure are detailed in the subsections below.

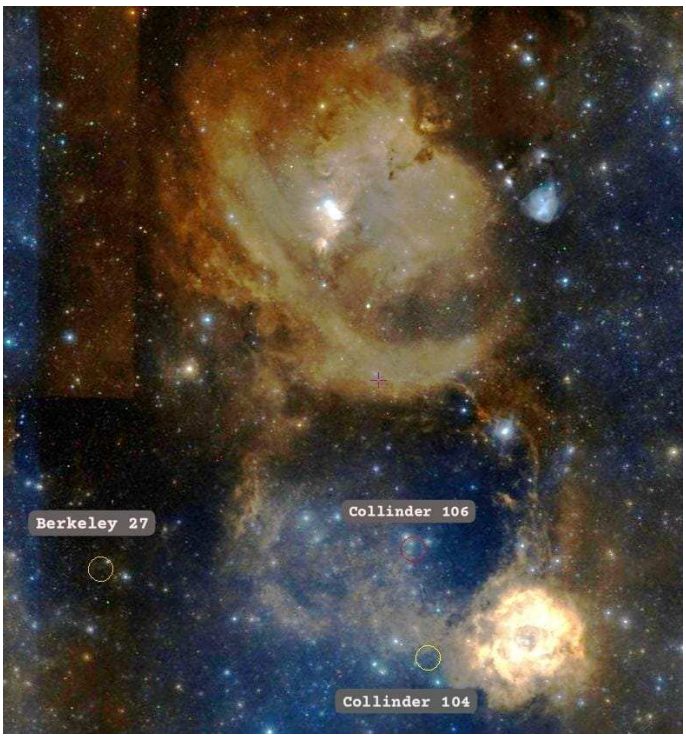

FIGURE 1: Monoceros region with circles highlighting the objects of this study: Berkeley 27 (orange), Collinder 104 (yellow), and Collinder 106 (red).

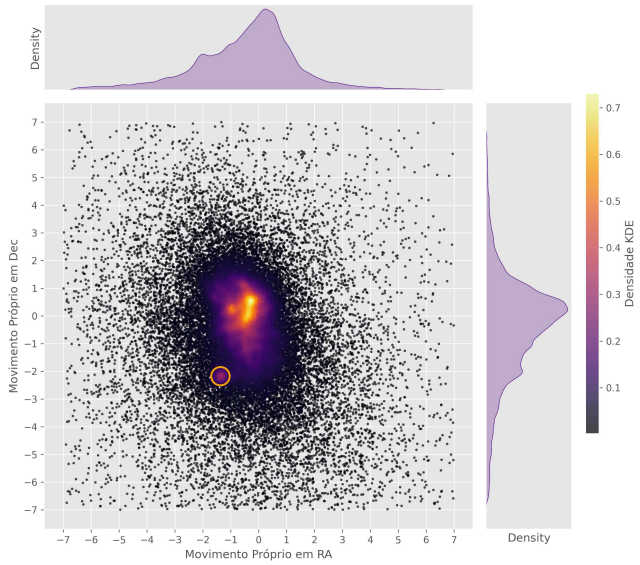

FIGURE 2: VPD showing an overdensity corresponding to the stars with similar proper motion, that might be assigned as cluster members.

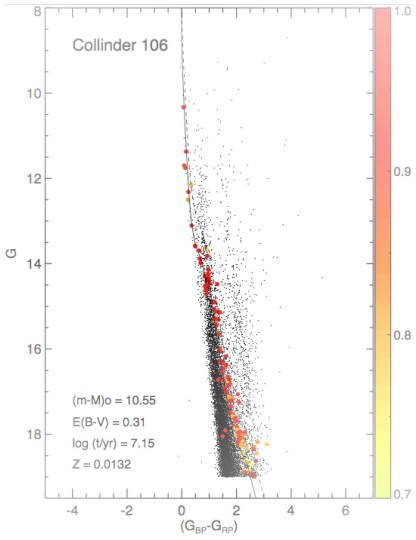

FIGURE 3: Decontaminated CMD where the colors represent the membership likelihood. The continuous lines are PARSEC isochrones fitted to the data of the cluster.

2.1.1. *Pre-analysis: finding the signature of a cluster*

In the first step, we have inspected the dispersion of the data in their Color-Magnitude Diagrams (CMDs) and Vector-Point Diagrams (VPDs) with $G \leq 19mag$ and $G_{BP} - G_{RP} \leq 2.0$ to identify the overdensities (see Figure 2) that correspond to stars with similar proper motions and to obtain the central coordinates, proper motion and parallax, as described in Ferreira et al. (2020).

With the coordinates of the center (RA and DEC) and proper motion mean values μ_α, μ_δ, we have built a radial density profile (RDP) to estimate the size of each object.

2.1.2. *CMD Decontamination, isochrone fitting, and structural parameters*

To derive membership for the stars, we have applied a routine that evaluates statistically the overdensities of the cluster stars in comparison to those in a nearby field within the 3D astrometric space (μ^*_α, μ_δ and ϖ), as described in Angelo et al. (2019).

We have employed solar metallicity PARSEC-COLIBRI models to perform isochrone fittings on the decontaminated CMD (see Figure 3) aiming to determine the true distance modulus $(m-M)_0$, $E(B-V)$ colour excess, age ($log(t/yr)$) the metalicities ($[Fe/H]$), for each object.

Structural parameters: core (r_c) and tidal (r_t) radii, have been obtained by King King (1962) model fittings, using a MCMC algorithm (see Figure 4).

2.1.3. *Total Mass*

A direct summation of the masses of star members has been made adopting, as the mass of each star, the mass of the nearest point on the fitted isochrone through interpolation routines and the k-nearest neighbors algorithm. The total mass of the cluster has been determined from the integrated magnitude, calculated by summing the flux from member stars, along with the age of the cluster Maia et al. (2014):

$$\log \mathcal{M} = a + b \log t - 0.4(M_G - M_{G,\odot}) \quad (1)$$

where $a = -6.09$, $b = 0.644$ and $M_{G,\odot} = 4.67$.

The values obtained for the clusters are listed in Table 1. Cluisters with just one value represent those where the mass function could not be constructed due to the limited number of member stars identified.

2.2. SOAR

The photometric data analyzed in this work were obtained with the SOAR Telescope using the Strömgren $uvby$ system, in Goodman Spectrograph (see Table 2). The data reduction and

TABLE 1: Physical and astrometric parameters of the studied clusters. When two mass values are listed, the first corresponds to the mass estimated from the mass function, while the second was obtained from the integrated mass function.

Aglomerados	RA	Dec	pmRA	pmDec	Parallax	$\log(t/\mathrm{yr})$	$E(B-V)$	$(m-M)$	Z	Massa ($M_\odot$)
Collinder 104	99.18	4.99	-1.36	0.61	0.63	7.20	0.75	10.62	0.0112	143
Collinder 106	99.29	6.05	-1.55	0.55	0.62	7.15	0.31	10.55	0.0132	151 / 121
Berkeley 27	102.84	5.79	-1.04	0.14	0.25	9.30	0.32	13.50	0.0120	446
NGC 2301	102.93	0.44	-1.35	-2.18	1.15	8.30	0.07	9.60	0.0172	540 / 422

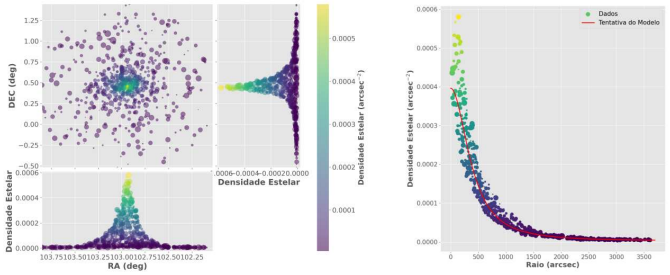

FIGURE 4: Left: Sky chart showing the initial stellar density calculated from the data sample. Right: Initial model fit to the radial profile of the cluster.

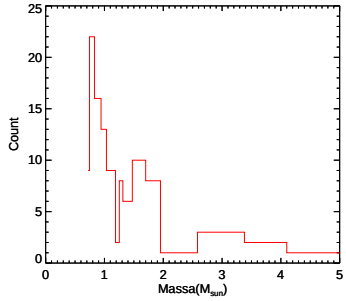

FIGURE 5: Histogram illustrating the density of different mass values for Collinder 106. The cluster's member stars have masses below 2 solar masses, in their majority.

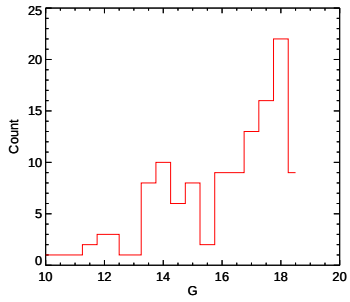

FIGURE 6: Histogram illustrating the mass distribution of the cluster based on magnitudes. It is evident that the density of stars with low magnitude is higher than the number of stars with high magnitude.

TABLE 2: Observed clusters, their positions, and observing nights.

Cluster	α **(J2000)**	δ **(J2000)**	**Observing Night**
Collinder 104	06:36:26.9	+04:46:23	2022-12-18
Collinder 106	06:37:06.7	+06:00:07	2022-12-12 2024-11-28 2024-12-28 2025-01-25
Berkeley 27	06:51:20.0	+05:46:19	2022-12-18
NGC 2301	06:51:43.22	+00:26:54.80	2021-12-12

calibration procedures followed standard techniques and are summarized below.

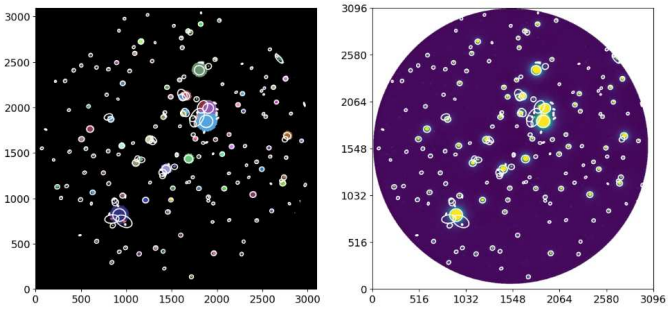

FIGURE 7: Aperture photometry process applied to the detected sources.

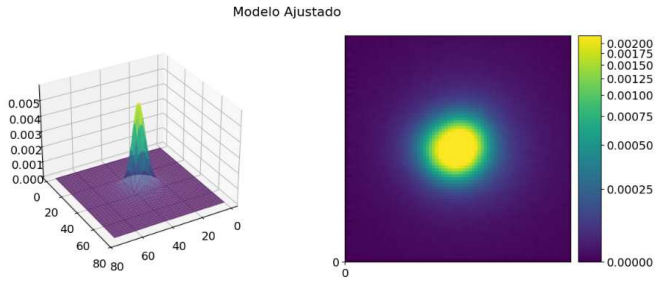

FIGURE 8: PSF model used for stellar profile fitting. The left panel shows a three-dimensional representation of the PSF surface. The right panel displays a top-down view (2D projection).

2.2.1. *Pre-processing*

The raw images were pre-processed using master calibration frames in order to correct for instrumental effects. Master bias frames were used to remove the electronic offset of the detector, while master flat-field frames were applied to correct for pixel-to-pixel sensitivity variations across the CCD. These steps ensure a uniform photometric response over the entire field of view.

2.2.2. *Photometry*

Stellar detection and photometric measurements were performed using both aperture and point spread function (PSF) photometry. Aperture photometry was initially employed to identify sources and obtain preliminary instrumental magnitudes (see Figure 7).

Subsequently, PSF photometry was applied to improve the photometric precision, particularly in regions with higher stellar density, resulting in more accurate instrumental magnitudes for the detected stars (see Figure 8 and Figure 9).

2.2.3. *Atmospheric Extinction Correction*

Atmospheric extinction corrections were applied independently for each Strömgren filter. The extinction coefficients (k_u, k_v, k_b,

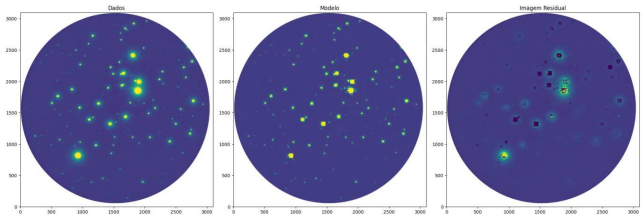

FIGURE 9: Detected sources based on the PSF model (center), shown alongside the original image of the cluster (left) and the residual image after model subtraction (right).

TABLE 3: Atmospheric extinction coefficients derived for the processed observing nights.

Night	k_u	k_v	k_b	k_y
12/12/2021	0.51 ± 0.02	0.27 ± 0.01	0.16 ± 0.01	0.04 ± 0.01
18/12/2022	0.54 ± 0.06	0.33 ± 0.07	0.26 ± 0.05	0.13 ± 0.02

and k_y) were determined from observations of the open cluster NGC 2301, which was observed at different airmasses during each night. The instrumental magnitudes were corrected according to the relations:

$$u_i = u_0 + k_u x \qquad v_i = v_0 + k_v x \tag{2}$$
$$b_i = b_0 + k_b x \qquad y_i = y_0 + k_y x \tag{3}$$

where the subscript i denotes the observed magnitude at a given airmass x, and the subscript 0 represents the magnitude corrected to zero airmass.

At the time of this analysis, only two of the observed nights have been fully processed. The atmospheric extinction coefficients derived from these nights are listed in Table 3.

2.2.4. *Transformation to the Standard System*

After correcting for atmospheric extinction, the instrumental magnitudes were transformed to the standard Strömgren system using linear calibration equations. The transformations include color terms to account for differences between the instrumental and standard photometric systems and are given by:

$$V_{\rm std} = A + B(b-y)_{\rm std} + y_{0i}, \tag{4}$$
$$(b-y)_{\rm std} = C + D(b-y)_{0i}, \tag{5}$$
$$m_{1,\rm std} = E + Fm_{1,0i} + J(b-y)_{\rm std}, \tag{6}$$
$$c_{1,\rm std} = G + Hc_{1,0i} + I(b-y)_{\rm std} \tag{7}$$

where A, B, C, D, E, F, G, H, I, and J are the calibration coefficients determined from standard stars observed during the same nights. The resulting magnitudes and color indices are therefore placed onto the standard Strömgren photometric system (see Figure 10).

Figure 11 shows the color–magnitude diagrams (CMDs) obtained from calibrated Strömgren photometric data acquired with the SOAR Telescope for the studied clusters. Unfortunately, the data obtained in 2021 for the Collinder 106 cluster did not present sufficient quality to be used, due to unfavorable atmospheric conditions.

3. Conclusions

The derived astrophysical parameters for NGC 2301 show good agreement with previous studies, validating the adopted methodology. In addition, the masses of Collinder 104, Collinder 106, and Berkeley 27 have been derived for the first time in this work.

A key outcome of the Strömgren photometric analysis is the development of a reproducible data-reduction methodology, supported by Python-based tools for the processing and calibration of the photometric data. This framework provides a solid basis for the analysis of the remaining observations.

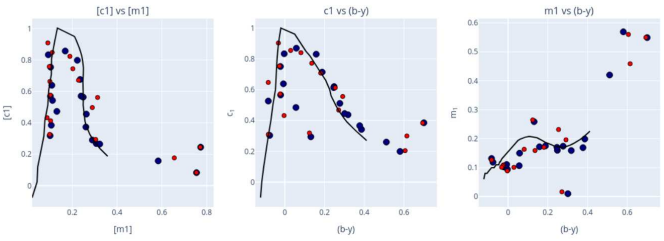

FIGURE 10: Diagrams showing the calibrated indices of the stars (in red) overploted on their corresponding literature values (in blue), demonstrating the effectiveness of the photometric calibration process.

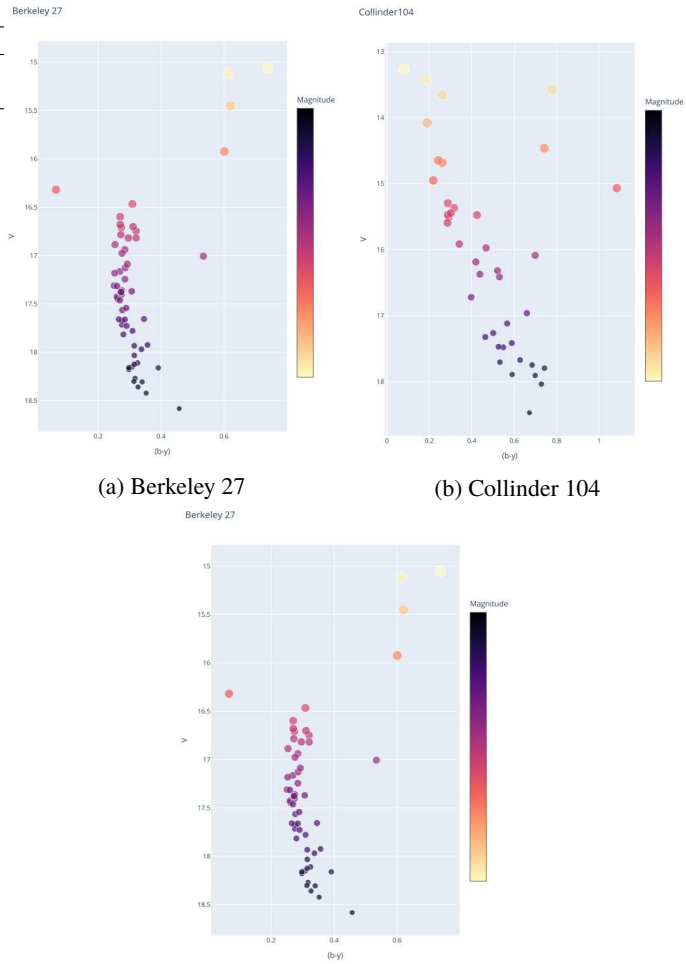

(a) Berkeley 27 (b) Collinder 104

(c) NGC 2301

FIGURE 11: Color–magnitude diagrams (CMD) obtained from calibrated Strömgren photometry with the SOAR Telescope. The plot shows the V magnitude as a function of the (b-y) color index for the clusters Berkeley 27 (a), Collinder 104 (b), and NGC 2301 (c).

The Strömgren *uvby* photometric data obtained with the SOAR Telescope between 2021 and 2025 will continue to be processed in order to derive the reddening-free indices $[c_1]$ and $[m_1]$. These indices will enable an independent determination of the metallicity, based on the calibration of Casagrande et al. (2011), and will contribute to improved cluster membership determination and more reliable isochrone fitting. The continued application of the developed methodology is expected to lead to a refined metallicity analysis for the studied clusters.

Acknowledgements. The authors wish to thank the support of UFMG, LNA, CEFET-MG and UFRJ.

References

Angelo, M. S., Santos, J. F. C., Corradi, W. J. B., & Maia, F. F. S. 2019, A&A, 624, A8
Babusiaux, C., Fabricius, C., Khanna, S., et al. 2023, A&A, 674, A32
Casagrande, L., Schönrich, R., Asplund, M., et al. 2011, A&A, 530, A138
Dias, W. S., Monteiro, H., Moitinho, A., et al. 2021, MNRAS, 504, 356
Ferreira, F. A., Corradi, W. J. B., Maia, F. F. S., et al. 2020, MNRAS, 496, 2021
Hunt, E. L. & Reffert, S. 2023, A&A, 673, A114
Jaehnig, K., Bird, J., & Holley-Bockelmann, K. 2021, ApJ, 923, 129
Kaltcheva, N., Kuchera, A., & Hathaway, C. 2010, Astron. Nachr., 331, 384
King, I. 1962, AJ, 67, 471
Krumholz, M. R., McKee, C. F., & Bland-Hawthorn, J. 2019, ARA&A, 57, 227
Maia, F. F. S., Piatti, A. E., & Santos, J. F. C. 2014, MNRAS, 437, 2005
Piatti, A. E., Pietrzyński, G., Narloch, W., et al. 2019, MNRAS, 483, 4766
Tarricq, Y., Soubiran, C., Casamiquela, L., et al. 2022, A&A, 659, A59